Accelerating Maximal Quasi-Clique Mining using GPUs

Michael Greenbaum
Rowan University
Glassboro, NJ, USA
greenb88@students.rowan.edu

Guimu Guo
Rowan University
Glassboro, NJ, USA
guog@rowan.edu

***Abstract*—The exploration of maximal quasi-cliques (MQC) within graphs is a computationally intensive problem (NP-hard) with wide-ranging applications in social network analysis, bioinformatics, and network security. The massive parallelism in graphics processing units (GPUs) is well suited for solving maximal quasi-cliques mining. However, it is a challenge to parallelize the quasi-clique algorithm on the GPU due to (i) the redesign of 6 pruning rules by utilizing a GPU-aware data structure following coalesced memory access, (ii) the enormous memory requirement of current approaches, and (iii) the drastic load imbalance among different tasks and the efficient utilization of threads and blocks. In this paper, we propose cuQC, the first GPU-accelerated approach designed to efficiently mine MQC, leveraging the parallel processing capabilities of modern GPUs. The cornerstone of our approach is developing an innovative data structure optimized for GPU memory hierarchy, facilitating rapid access and manipulation of graph data. Our experimental evaluation demonstrates the efficacy of our approach by comparing the execution time and graph size that can be handled against the state-of-the-art CPU implementations. Our source code is released at https://github.com/Mike12041204/cuQC.**

I. Introduction

The discovery of dense subgraphs from one big graph has attracted increasing attention. One notable dense structure is γ-quasi-clique, which is a natural generalization of a clique that is useful in mining various networks [1]. Specifically, given a degree threshold γ and an graph G, a γ-quasi-clique is a subgraph of G, denoted by $g = (V_g, E_g)$, where each vertex connects to at least $\lceil \gamma \cdot (|V_g| - 1) \rceil$ other vertices in g [2], [3].

Detecting small quasi-cliques often yields trivial insights and is not considered valuable. Maximal quasi-cliques (MQC), on the other hand, are critical in graph analysis. A MQC is a specific type of γ-quasi-clique that cannot be extended further by adding more vertices from the graph while maintaining its density threshold γ. Enumerating all MQCs within a graph that meet or exceed a specified minimum vertex count threshold τ_{size} is a significant computational challenge.

MQC mining is extensively applied in a variety of domains, such as identifying functional modules or protein complexes in biological networks [4]–[9], uncovering communities within social networks [10], [11], identifying spam/phishing email sources [12], [13], conducting digital forensics [14], etc.

Challenges and Existing Methods. The problem of finding all MQCs in a graph is NP-Hard [15], [16]. Even determining whether a given quasi-clique is maximal is already NP-hard. This high computational complexity arises from the need to explore potentially vast numbers of vertex subsets to identify those that satisfy the quasi-clique criteria. This becomes increasingly challenging as graphs can be extremely large in real-world applications.

Several algorithms have been proposed for mining γ-quasi-cliques, including Crochet [17], [18], Cocain [19], and Quick [3]. These algorithms generally use a depth-first order to explore the search space (i.e., the set of all possible vertex sets), incorporating pruning techniques that eliminate vertices from consideration if they cannot possibly form a quasi-clique satisfying the density criteria. Despite sophisticated pruning techniques, these state-of-the-art algorithms [3], [17], [19] are unable to scale to large datasets. For example, Quick [3] can only handle graphs with thousands of vertices. This limitation leads quasi-clique mining research to focus on developing heuristic algorithms that can provide practical solutions under specific conditions [15]. Besides this, γ-quasi-clique mining does not satisfy the hereditary property (i.e., a subgraph of a γ-quasi-clique is not always a γ-quasi-clique). The advanced techniques that have been developed for enumerating subgraphs that satisfy the hereditary property (e.g., k-plexes, s-defective cliques, etc.) cannot be utilized [20].

Since MQC mining involves exploring numerous combinations of vertices and edges, following the divide and conquer paradigm, the problem of mining a big graph can be partitioned into tasks that mine smaller subgraphs concurrently. Owing to the massive parallel processing capabilities, high bandwidth, and low power requirements, GPUs are well suited for solving the MQC mining problem in big graphs, where the sheer volume of data and the number of potential subgraphs to analyze can be overwhelming for traditional CPUs. However, achieving high performance for mining MQCs on GPUs presents several challenges:

- *Irregular Memory Access Patterns*: The pruning techniques, such as the diameter-based pruning (cf. Section II), along with updating vertex degrees following a pruning event, necessitate the intersection of sets of vertices and their neighbors. The neighbors for the intersection might not be in contiguous memory, leading to non-sequential memory accesses. These functions, characterized by irregular memory access patterns, are the main time-consuming operation of the program.

- *Memory Limitations*: GPUs have limited onboard memory, which can pose a significant constraint when dealing with big graphs. Besides, effectively managing the GPU's different memory types—global, shared, and registers—is challenging yet crucial for performance optimization, given their varying sizes, speeds, and access patterns.
- *Highly Imbalanced Workload*: The number of nodes in each subgraph and the neighbors of different nodes can vary significantly, resulting in a substantial workload imbalance. Addressing these imbalances requires multi-level solutions, spanning warps, thread blocks, and grids, further complicating the issue.

Our **contributions** are summarized below:

- We propose a high-throughput algorithm designed for parallel execution, incorporating various pruning strategies optimized for the GPU architecture.
- We introduce novel task data structures to facilitate highly concurrent memory accesses. A dynamic task scheduling approach and a warp-level intersection technique have been crafted to ensure balanced workload distribution. Finally, a task cache mechanism has been devised to control the rate at which tasks are spawned, ensuring memory utilization remains bounded.
- We employ various optimization techniques to amplify their effectiveness on GPU, including a hybrid CPU-GPU approach, a shared memory buffer, and a single-pass expansion procedure.
- We developed a distributed memory version of the algorithm that leverages multiple GPUs, enabling the handling of larger graphs at enhanced processing speeds.
- We compare the above algorithms against the state-of-the-art approaches comprehensively, using 21 public graph datasets of various characteristics.

II. PRELIMINARIES

A. Definitions

Graph Notations. We consider an undirected graph $G = (V, E)$, where V (resp. E) is the set of vertices (resp. edges). The vertex set of a graph G can also be explicitly denoted as $V(G)$. Given $S \subseteq V$, we use $G(S)$ to denote the subgraph of a graph G induced by S, which includes a subset of the vertices of $V(S)$ together with any edges whose endpoints are all in this subset. $|S|$ is the number of vertices in S.

Given $v \in G$, $N(v)$ denotes the set of neighbors of v in V. We further define $d(v) = |N(v)|$ as the degree of v in G. Given a vertex subset $V' \subseteq V$, we define $N_{V'}(v) = \{u \,|\, (u, v) \in E, u \in V'\}$, i.e., $N_{V'}(v)$ is the set of v's neighbors inside V', and we also define $d_{V'}(v) = |N_{V'}(v)|$.

Problem Definition. Next, we formally define our problem.

Definition 1 (γ-quasi-clique): A graph $G = (V, E)$ is a γ-quasi-clique ($0 < \gamma \leq 1$) if G is connected, and for every vertex $v \in V$, its degree $d(v) \geq \lceil \gamma \cdot (|V| - 1) \rceil$.

Definition 2 (Maximal γ-quasi-clique): A γ-quasi-clique $G(S)$ is maximal if and only if there is no other γ-quasi-clique $G(S')$ containing $G(S)$, i.e., $S \subset S'$.

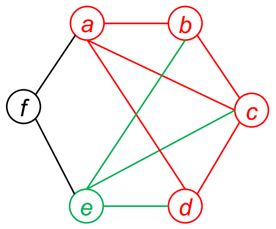

Fig. 1. An Illustrative Graph

To illustrate using Fig. 1, consider $S_1 = \{v_a, v_b, v_c, v_d\}$ (i.e., vertices in red) and $S_2 = S_1 \cup v_e$. If we set $\gamma = 0.6$, then both S_1 and S_2 are γ-quasi-cliques: every vertex in S_1 has at least 2 neighbors in $G(S_1)$ among the other 3 vertices (and $2/3 > 0.6$), while every vertex in S_2 has at least 3 neighbors in $G(S_2)$ among the other 4 vertices (and $3/4 > 0.6$). Also, since $S_1 \subset S_2$, $G(S_1)$ is not a maximal γ-quasi-clique. But graph G, as a whole, is not a 0.6-quasi-clique as v_f only has 2 neighbors among the other 5 vertices ($2/5 < 0.6$). If a graph is a γ-quasi-clique, its subgraphs usually become uninteresting, so we only mine maximal γ-quasi-cliques in this paper.

Small γ-quasi-cliques are also trivial and not interesting. For example, a single vertex or an edge with two end-vertices are quasi-cliques for any γ. In the literature of dense subgraph mining, researchers usually only strive to find large subgraphs. These state-of-the-art algorithms [2], [3] used the minimum size threshold τ_{size} to filter small quasi-cliques.

Definition 3 (Problem Statement): Given a graph $G = (V, E)$, a minimum degree threshold $\gamma \in (0, 1]$ and a minimum size threshold τ_{size}, we aim to find all the vertex sets S such that $G(S)$ is a maximal γ-quasi-clique of G, and that $|S| \geq \tau_{size}$.

For a smaller value of γ, there exist numerous γ-quasi-cliques, yet the majority of them are of small size and not cohesive. γ-quasi-clique follow the property that for $\gamma \geq 0.5$, the diameter of a γ-quasi-clique is at most 2 [17]. In previous studies [2], [3], [18], it was a convention to set the $\gamma \geq 0.5$, although it is also possible to calculate the diameter's limit when $\gamma < 0.5$ using the Theorem 1 in [17]. This property can be used to remove vertices early from the candidate set that are not 2-hops away from the vertices already in the result set. Following [2], [3], [18], we focus on those γ-quasi-clique with $\gamma \geq 0.5$ only in this paper.

B. GPU Architecture

The nature of MQC mining involves exploring large numbers of potential subgraphs, which can be handled in parallel. GPUs are ideal for the iterative and data-intensive tasks involved in MQC mining.

Streaming Processors. In GPU architecture, 32 threads form a warp, executing instructions uniformly. In particular, the GPU executes one warp of threads in a Single Instruction Multiple Data (SIMD) fashion. Warps compose a thread block assigned to a streaming multiprocessor (SM) equipped with execution units, L1 cache/shared memory, and registers. A GPU contains several SMs, and each SM contains hundreds of CUDA cores. Multiple blocks constitute a grid, correlating to a kernel launch, executed across several SMs, optimizing parallel task processing. The workload of different threads should be balanced because an imbalanced workload among threads will lead to severe thread divergence.

GPU Memory Architecture. Registers are the fastest in the GPU memory hierarchy and are allocated per thread. Threads in a warp can efficiently swap data using warp-level primitives that utilize registers. A shared L1 cache/memory is accessible to threads within the same block and is programmable but with limited space. It is best to keep the elements shared by the thread block in shared memory and keep thread-local data in registers. The entire GPU utilizes a shared L2 cache, with global memory atop it. Global memory has the slowest access rate but can be accessed by all threads. GPU threads cannot directly access the CPU memory, emphasizing the importance of CPU-GPU data movement and memory management strategies within the GPU's architecture.

Maximizing data reuse on the GPU for data-intensive tasks like MQC mining poses a significant challenge. We can improve efficiency if all the necessary data for the threads inside a warp can be obtained in a single memory transaction. This pattern is called *coalesced memory access*, i.e., all threads in the warp access consecutive memory addresses.

CUDA programming. CUDA (Compute Unified Device Architecture) is a parallel computing platform and programming model developed by NVIDIA for general computing on its GPUs. CUDA APIs leverage the parallel processing power of the GPU and facilitate efficient thread synchronization within blocks and warps. A key to utilizing CUDA is the ability to divide a task into smaller computing units that can be executed concurrently. This makes it particularly well-suited for applications requiring high throughput computations.

A kernel function launched by the GPU is specified in the form *kernel_function<<<BLK_NUM, BLK_DIM>>>*, where *BLK_NUM* is the number of thread blocks and *BLK_DIM* is the number of threads in each thread block. The GPU allows multiple threads to execute the same code specified by the body of the kernel function, but on different data. This data parallelism is realized because each thread has access to the following built-in variables in CUDA:

- *blockIdx.x:* the index of a block;
- *blockDim.x:* the number of threads in each block, aka. the block dimension, as specified by *BLK_DIM*;
- *threadIdx.x:* the thread index within a block;

In this paper, we generalize those built-in variables as below.

- For a particular thread, its warp ID in the block: *WARP_ID* = *threadIdx.x* / 32
- The ID of a thread in the warp: *LANE_ID* = *threadIdx.x* $\%$ 32

III. Related Work

A. The State-of-the-art Serial Algorithm

Existing research consistently utilizes a branch-and-bound (BB) strategy to enumerate MQCs. Their primary objective is to develop efficient pruning rules that narrow search space.

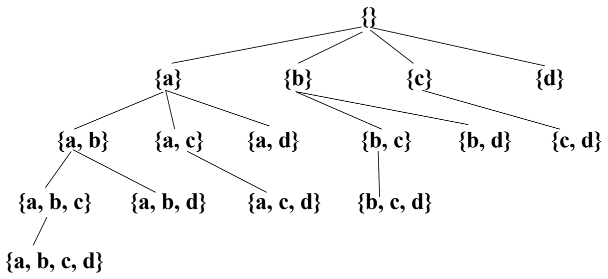

Fig. 2. Set-Enumeration Tree

The earliest BB algorithms proposed for MQC mining are Crochet [17], [18] and Cocain [19]. Subsequently, Quick [3] incorporates all prior pruning rules and implements additional novel pruning techniques, like upper-bound and lower-bound pruning. Quick+ [2], [21] has made additional improvements to the pruning rules in Quick and have handled certain boundary cases that were previously inadequately addressed.

We will take Quick+ as an example to provide a brief introduction to the BB algorithm. The giant search space of a graph $G = (V, E)$, i.e., V's power set, can be organized as a set-enumeration tree [3]. Fig. 2 shows the set-enumeration tree T for a graph G with four vertices $\{a, b, c, d\}$ where $a < b < c < d$ (ordered by ID). Each tree node represents a vertex set S, and only vertices larger than the largest vertex in S are used to extend S. For example, in Fig. 2, node $\{a, c\}$ can be extended with d but not b as $b < c$; in fact, $\{a, b, c\}$ is obtained by extending $\{a, b\}$ with c.

Quick+ recursively partitions the search tree into multiple subtrees via branching. Let us denote T_S as the subtree of the set-enumeration tree T rooted at a node with set S. Then, T_S represents a search space for all possible γ-quasi-cliques that contain all vertices in S. In other words, let Q be a γ-quasi-clique found by T_S, then $Q \supseteq S$.

Quick+ represents the task of mining T_S as a pair $\langle S, ext(S)\rangle$, where S is the set of vertices assumed to be already included, and $ext(S) \subseteq (V - S)$ keeps those vertices that can extend S further into a γ-quasi-clique. Many vertices cannot form a γ-quasi-clique together with S and can thus be safely pruned from $ext(S)$; therefore, $ext(S)$ is usually much smaller than $(V - S)$. Specifically, Quick+ starts from the universal search space $\langle S, ext(S)\rangle$, where $S = \emptyset$ and $ext(S) = V$.

Note that the mining of T_S can be recursively decomposed into the mining of subtrees rooted in the children of node S in T_S, denoted by $S' \supset S$. Since $ext(S') \subset ext(S)$, the subgraph induced by nodes of a child task $\langle S', ext(S')\rangle$ is smaller.

During the recursive branching process, Quick+ applies two types of pruning techniques, namely Type I pruning rules and Type II pruning rules. Type I pruning rules are conducted on $ext(S)$ and aim to refine $ext(S)$ by removing those vertices that satisfy certain conditions; Type II pruning rules are conducted on S and aim to prune those branches where vertices in S satisfy certain conditions. The rationale is that if a vertex v satisfies certain conditions, each MQC covered by this branch should not include this vertex. Thus, we can either remove v from $ext(S)$ for this branch, i.e., Type I pruning rules apply (if $v \in ext(S)$), or prune the entire branch, i.e., Type II pruning rules apply (if $v \in S$). For simplicity, we omit the details of these pruning techniques and refer to [2].

This set-enumeration approach typically requires postprocessing to remove non-maximal quasi-cliques from the set of valid quasi-cliques found [3]. For example, when processing a task that mines $T_{\{b\}}$, vertex a is not considered. Thus the task has no way to determine that $\{b, c, d\}$ is not maximal, even if $\{b, c, d\}$ is invalidated by $\{a, b, c, d\}$ which happens to be a valid quasi-clique, as $\{a, b, c, d\}$ is processed by the task mining $T_{\{a\}}$. But this post-processing is efficient, especially when the number of valid quasi-cliques is not big (as we only find large quasi-cliques).

B. Parallel Solution

Other than the top-k quasi-clique algorithm [15], quasi-cliques have seldom been considered in a big graph setting. Quick [3] was only tested on two small graphs: one with 4,932 vertices and 17,201 edges, and the other with 1,846 vertices and 5,929 edges. With the goal of scaling to big graphs, parallel computing techniques have been widely used to solve the graph mining problem. Several subgraph-centric systems have been proposed to solve graph mining problems, including NScale [22], Arabesque [23], G-Miner [24] and G-thinker [25]. These parallel approaches involve partitioning the search set-enumeration tree in Fig. 2 into subtrees and executing the branch-and-bound algorithm on each subgraph in parallel. To ensure a high task throughput, G-thinker [25] proposes a CPU-bound system that overlaps communication with computation to minimize CPU idle time. Building upon G-thinker, Quick+ [2] has been developed to address the problem of mining maximal cliques. Despite these advancements in parallel CPU systems, GPU-based solutions for MQC mining remain unexplored. This paper introduces the first GPU-accelerated approach to confront this challenge.

IV. Design of cuQC

In this section, we present the design of our high-performance MQC algorithm for the GPU.

A. Overview and Challenges

Task Based Design. Our algorithm follows the branch-and-bound algorithm framework of Quick+ [2] as introduced in Section III-A. We partition the set-enumeration tree and each subtree is encapsulated as a task, presented as a pair $\langle S, ext(S)\rangle$. Thus, every task can be accessed independently, enabling parallelism that was not possible in Quick's [3] recursive approach. Note that in Fig. 3, for simplicity, only the vertices in S are used to represent the tasks. In each level of the enumeration tree, tasks are stored consecutively in a *TaskList* and differentiated using various highlights in Fig. 3.

The first challenge is to determine the proper smallest computing unit for parallelism. In the parallel CPU program, Quick+ on T-thinker [21], the computing unit is a CPU thread. On the GPU, a warp consisting of 32 threads is a more suitable choice as it facilitates coalesced memory access of adjacency

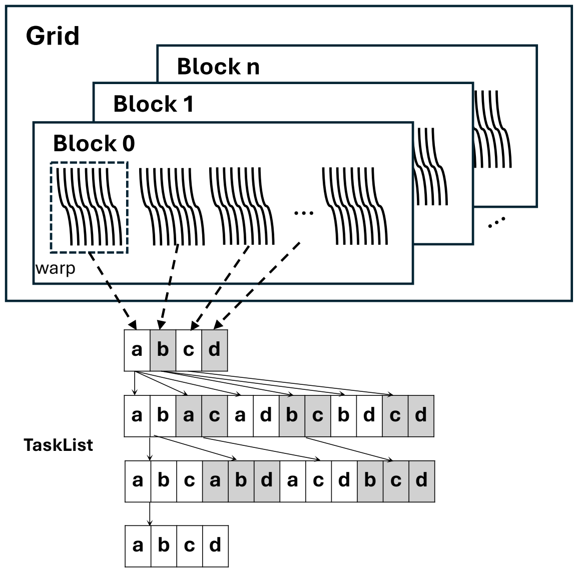

Fig. 3. Warp Task Assignment

lists. The majority of operations in an MQC mining task involve the examination of vertex sets or the intersection of adjacency lists (to be described in Section IV-C). As shown in Fig. 3, we assign each warp to handle one task (which corresponds to a node in the set-enumeration tree shown in Fig. 2). Every thread in the warp runs the related operations in parallel, such as updating the degree for all v's neighbors when moving v from candidate set $ext(S)$ to S. This representation and generation of numerous independent warp-oriented tasks allows for effective utilization of the GPU.

B. Data Structure

Graph Data Structure. We store the graph $G = (V, E)$ in the global memory compactly using a compressed sparse row (CSR) format [26], [27]. Please refer to Figure 2 in [26] as an example. Our graph data structure includes 4 arrays:

- *OneHopAdj* (resp. *TwoHopAdj*): the concatenation of the one-hop (resp. two-hop) adjacency lists;
- *OneHopOffset* (resp. *TwoHopOffset*): the start location of the neighbor list of vertex i in *OneHopAdj* (resp. *TwoHopAdj*);

Task Data Structure. The real information of each task is prepared in CSR format (as shown in Fig. 4). We keep these tasks in the global memory compactly as 6 arrays:

- *taskOffset*: *taskOffset[i]* represent the start location of task i in the *vertices* array;
- *vertices*: all vertices in $\langle S, ext(S)\rangle$ of each task;
- *label*: for vertex *vertices[i]*, *label[i]* identifies its corresponding status. 0 means *vertices[i]* is in S, 1 means it is in *ext(S)*, 2 means being covered (see IV-G), and -1 means being pruned;
- *indeg*: the number of neighbors that *vertices[i]* has in S, i.e. *indeg[i]* = $|N_S($*vertices[i]*$)|$;
- *exdeg*: the number of neighbors that *vertices[i]* has in $ext(S)$, i.e. *exdeg[i]* = $|N_{ext(S)}($*vertices[i]*$)|$;

- *lvl2adj*: *lvl2adj[i]* = number vertices in *ext(S)* which are within 2-hops from *vertices[i]*;

As shown in Fig. 4, suppose we have 3 tasks from a fully connected graph {a,b,c,d}. T_1 has $\langle S_1, ext(S_1)\rangle = \{(a,b),(c,d)\}$; T_2 has $\langle S_2, ext(S_2)\rangle = \{(b,c),(d)\}$; T_3 has $\langle S_3, ext(S_3)\rangle = \{(c,d),\emptyset\}$. Then, these 3 tasks' required information will be represented as the 6 arrays in Fig. 4. This array-based data structure is ideal as direct index access allows each warp to read its tasks in parallel.

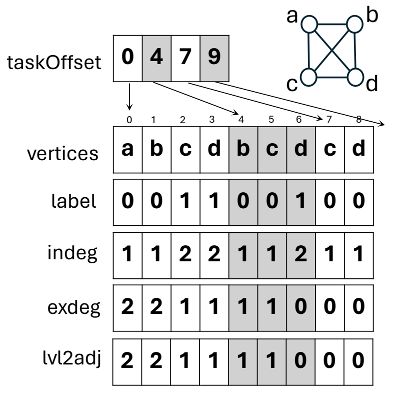

Fig. 4. Task Structure

C. GPU Algorithm

Host Program. The host program is presented in Algorithm 1. Line 1 loads the input graph into the main memory utilizing the CSR structure. Line 2 then executes an initial round of cover pruning (see Section IV-G). The covered vertices are exempt from spawning in Line 3 (status being marked in the label array). This ensures each vertex initiates a task following the specific data structure in Fig. 4.

Given that tasks correspond to subtrees spawned from the nodes in the set-enumeration tree depicted in Fig. 2, it is evident that the number of tasks is quite small initially. Consequently, it is not optimal to offload these preliminary tasks to the GPU, as their limited quantity would not fully utilize the GPU's computing power, leaving most of the GPU cores idle. Therefore we have variable *cpu_round* initialized to 0 in Line 4 to track the number of rounds executed on the CPU. With a hybrid CPU-GPU implementation strategy, the tasks will be transitioned to GPU processing only after exceeding the number of rounds specified by hyperparameter τ_{cpu}. Lines 5–10 execute the CPU *expand(t)* function as Quick+ introduced in Section III-A.

From Line 11 onwards, the program shifts to GPU execution. Line 11–12 prepare the required task data structures as Fig. 4 on GPU and copy the tasks from the CPU main memory to the GPU memory. As shown in Fig. 5 the task are stored in *TaskList* and *TaskBuffer* (an auxiliary container to control task spawning speed, cf. Section IV-D). In Lines 13–20, each task is processed by one warp until both the *TaskList* and *TaskBuffer* on GPU are empty. Notably, Line 14 invokes the *gpu_expand(t)* kernel function, where each warp expands an individual task into new tasks, applying pruning techniques to narrow down the search space for each new task. These new tasks are temporarily stored within the *WarpTaskBuffer* (see Fig. 5), to avoid the inefficiency of duplicated two-pass computations (detailed in Section IV-D). Upon completion of a round, once all tasks have been written to the *WarpTaskBuffer* by warps, Line 15 triggers the *transfer()*. This function transfers the newly expanded tasks back to the *TaskList*, or to the *TaskBuffer* if capacity constraints necessitate. Line 16 ensures the replenishment of tasks from *TaskBuffer* to *TaskList* to maintain warp occupancy. Throughout the execution of *gpu_expand(t)*, all valid quasi-cliques are stored in the GPU global memory in *ResultList*. Line 19 transfers results from *ResultList* to the host.

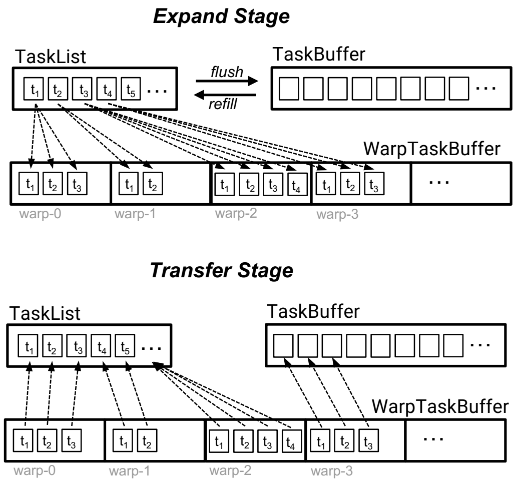

Fig. 5. Expand and Transfer

Kernel Program. Algorithm 2 shows an *expand* kernel, where the tasks are distributed to the warps for further expansion and pruning. Initially, to read tasks from *TaskList* in parallel by warps on GPU, we maintain a cumulative counter, *global_count*, to track the next task to be processed. In Lines 1–3, each warp localizes the next task in *TaskList* and increments the *global_count* by one. Lines 4–30 repeatedly expand current task, employ pruning strategies to reduce the search space, verify the validity, and retrieve the next tasks.

Specifically, Lines 6–12 perform the lookahead pruning to verify if the entire $S \cup ext(S)$ collectively satisfies the criteria for a γ-quasi-clique. Subsequently, Line 14 move one vertex v from the candidate set $ext(S)$ to S. Given the constraint $\gamma \geq 0.5$, all the vertices must be within 2-hops to form a γ-quasi-clique (see Section II). Line 15 removes vertices from the candidate set that are not within 2-hops of v. To fully leverage the high-speed shared memory, the new task with $\langle S', ext(S')\rangle$ will be stored in shared memory if $|S'| < \tau_{shared}$, or stored in global memory. τ_{shared} is a hyperparameter defined by users according to their GPU hardware. Lines 16–18 engage in pruning the new tasks, employing multiple CUDA warp-level primitives to implement the specified pruning criteria. The pruning rules are classified into two categories: Type I aims to eliminate unpromising vertices from the candidate set, whereas Type II can terminate exploration on the current task as demonstrated in Lines 19–21

Algorithm 1 GPU-Based MQC Algorithm: Host Program

```
Input: $G = (V, E)$
Output: All MQCs
1: Load Graph G into the host memory
2: Select cover vertex $u$ with the greatest degree
3: Spawn tasks from $V - N(u)$ and save in task list $T$
4: $cpu\_round \leftarrow 0$
5: if $cpu\_round > \tau_{cpu}$ then
6:     for each task $t \in T$ do
7:         $expand(t)$
8:     end for
9:     $cpu\_round \leftarrow cpu\_round + 1$
10: end if
11: Allocate $TaskList$ in device memory
12: Copy task list $T$ from host to the device $TaskList$
13: while $TaskList \neq \emptyset$ and $TaskBuffer \neq \emptyset$ do
14:     Launch kernel $gpu\_expand(t)$
15:     Launch kernel $transfer()$
16:     if $|TaskList| < \tau_{expand}$ and $TaskBuffer \neq \emptyset$ then
17:         Refill from $TaskBuffer$ to $TaskList$
18:     end if
19:     Save $ResultList$ in file
20: end while
```

Algorithm 2 Kernel Function gpu_expand()

```
1: if $LANE\_ID = 0$ then
2:     $loc \leftarrow atomicAdd(global\_count, 1)$
3: end if
4: repeat
5:     $WarpTask \leftarrow TaskList[loc]$
6:     if $G(S \cup ext(S))$ is a $\gamma$-quasi-clique then
7:         Append $G(S \cup ext(S))$ to $ResultList$
8:         if $LANE\_ID = 0$ then
9:             $loc \leftarrow atomicAdd(global\_count, 1)$
10:        end if
11:        continue
12:    end if
13:    for each $v$ in $ext(S)$ do
14:        $S' \leftarrow S \cup v, ext(S) \leftarrow ext(S) - v$
15:        $ext(S') \leftarrow ext(S) \cap \{v's$ 2-hop-neighbors$\}$
16:        Warp-Level Degree-Based Pruning
17:        Warp-Level Lower- and Upper-Bound Based Pruning
18:        Warp-Level Critical Vertex Pruning
19:        if any of Type II pruning on $S'$ is triggered then
20:            continue
21:        end if
22:        Append new task $T_{\langle S', ext(S') \rangle}$ to WarpTaskBuffer
23:        if $S'$ is $\gamma - quasi - clique$ then
24:            append $S'$ to $ResultList$
25:        end if
26:    end for
27:    if $LANE\_ID = 0$ then
28:        $loc \leftarrow atomicAdd(global\_count, 1)$
29:    end if
30: until $loc \geq |TaskList|$
```

and detailed within Section IV-G. Lines 22–25 store new tasks in *WarpTaskBuffer* if they can be expanded further and check if the current S' is a γ-quasi-clique. Once all the candidates in this task have been explored, Lines 27–29 will localize the next task.

Another kernel function *transfer()* only transfers tasks and will be introduced in the Single-Pass Expansion Approach.

D. Approach

Task Flush and Refill. To manage memory usage, the system only computes a limited number of tasks to be expanded concurrently. If all available tasks are expanded at every level in the set-enumeration tree, memory usage may explode on big graphs. But, in terms of efficiency, maintaining a sufficient number of tasks in *TaskList* is also crucial to keep all warps busy. To control the task expansion rate, we introduce an expansion threshold τ_{expand}, which specifies the number of tasks planned for each level. Before expanding, if the number of tasks in *TaskList* is less than the τ_{expand}, we replenish it by transferring tasks from the *TaskBuffer*. During expansion, if the number of generated tasks exceeds the τ_{expand}, we flush the excess tasks from the *WarpTaskBuffer* to the *TaskBuffer* (see Fig. 5). Table VI in Section VII illustrates that τ_{expand} significantly impacts both the speed and memory consumption.

Hybrid CPU-GPU Approach. Ideally, once the program has loaded the input graph into memory, we could conduct all task processing and expansion on the GPU, leveraging its capacity for parallel processing. However, achieving this goal is hindered by a significant GPU memory constraint.

The size of tasks generated at lower levels of expansion is generally large, as less pruning has been done to each task. There will be a small amount of tasks, but each one will be exceptionally intensive. Directly running this small amount of heavy tasks on the GPU will introduce two issues: (1) workload imbalance, where most warps remain idle while a few are busy mining those heavy tasks (as discussed in Section IV-C), and (2) a significant increase in space demands due to these large early-stage tasks generating a huge amount of sub-tasks.

To address this problem, we consider running the first few levels on the CPU before moving to the GPU to minimize the *WarpTaskBuffer* size required by each warp. As mentioned in Section IV-C, users can control the transition point from CPU to GPU processing by adjusting the τ_{cpu} hyperparameter. We found switching after the second level gives the best performance for most cases. The hybrid CPU-GPU approach significantly decreases the memory required for expansion on the GPU allowing for the program to run on larger graphs.

Single-Pass Expansion Approach. Numerous GPU-based algorithms [28] take a two-pass approach when multiple threads need to write an unknown amount of heterogeneous output in parallel. The underlying logic of this two-pass method involves determining the size of each element during the first pass, followed by parallel output writing in the second pass. This principle is particularly applicable to parallel MQC mining. To get the writing location, it is essential to obtain the number and size of new tasks by executing a preliminary *expand* pass. Subsequently, a second *expand* pass is necessary to generate and store these new tasks in parallel.

As shown in Fig. 5, we developed a novel one-pass strategy utilizing an exclusive scan operation facilitated by the additional data structure *WarpTaskBuffer*. This structure preallocates buffers for each warp to write their partial results to. A device-wide synchronization is then performed after expansion to ensure the partial results generated by all warps are ready. Then the second kernel *transfer()* is launched that will transfer the data from *WarpTaskBuffer* to *TaskList* or *TaskBuffer* (depending on the capacity of *TaskList*). Hence, the kernel begins by assessing the size of tasks to be recorded in the *TaskList* to accurately determine the offset. We run an exclusive scan on the sizes to get the offsets. With the offsets, each warp will use its threads to transfer the data it generated to the *TaskList* and *TaskBuffer* in parallel as shown in Fig. 5.

The one-pass approach requires the additional calculation and synchronization of the *transfer()* kernel, but we have observed that this takes minimal time compared to the general *gpu_expand()* kernel call. As shown in our experiment, avoiding duplicate calculations leads to significant time savings.

E. Task Scheduling Approach

In many GPU-based graph mining algorithms [28], [29], an equal distribution of jobs across each computing unit is implemented. However, this approach of evenly allocating tasks to each warp leads to workload balancing issues when mining MQC. As demonstrated in [2], the runtime of MQC tasks varies significantly, and it is difficult to predict each task's runtime because of the complex pruning rules involved.

In this study, we implement a dynamic task scheduling approach, in contrast to the traditional method of statically allocating an equal number of tasks to each warp in advance. Instead, warps proactively fetch new tasks from *TaskList* upon completing their current ones. Our experiments indicate that this dynamic method significantly enhances performance.

F. Vertex Set in Shared Memory

The GPU consists of three types of memory: registers (the fastest but smallest), shared memory, and global memory (the largest but slowest). Tasks are composed of multiple frequently accessed vertices. For large tasks, storage in global memory is necessary, as registers and shared memory are very limited in size. However, shared memory access latency might be roughly 10 to 100 times faster than global memory access. To fully utilize the shared memory, within it, we allocate a buffer of size τ_{shared} called *SharedVertices* for each warp. During task expansion, newly generated tasks smaller than τ_{shared} will be stored in *SharedVertices*.

G. Pruning Rules

Our program utilizes the 6 pruning rules from Quick [3] to greatly reduce the search space of a graph.

- Diameter Pruning: given $\gamma \geq 0.5$, each time a vertex is added to the S from $ext(S)$, all vertices not within 2 hops of the new vertex can be eliminated.
- Degree-Based Pruning: it considers the minimum number of neighbors each vertex must have in the clique and whether that requirement is still achievable for each vertex. This pruning rule can be applied whenever the degrees of a vertex change.
- Cover Pruning: one vertex may have a strong connection with a group of other vertices, and they cannot form an MQC without including this key vertex. This vertex is referred to as a cover vertex in Quick [3], and the group of vertices it covers can be excluded from expansion.
- Lookahead Pruning: at the beginning of the expansion, we check whether the entire set forms a quasi-clique.
- Upper-lower Bound Pruning: it calculates the upper and lower bound on the number of vertices that can be added to S while maintaining the potential to form a MQC. With these refined bounds, additional degree-based pruning can be applied.
- Critical Vertex Pruning: A critical vertex in S is one for which all neighbors in the candidate set must be included to form an MQC. We identify these vertices and add all their neighbors.

More details of these pruning rules can be found in Quick [3]. These pruning rules all complement each other and are performed repeatedly. Without the use of all these rules analyzing larger graphs is impossible.

Example: Degree-Based Pruning. Adapting these pruning techniques on GPU necessitated innovative memory-management strategies. Due to space limitations, we cannot provide the GPU implementation details for each pruning technique. Instead, we use degree-based pruning as an example.

Degree-based pruning will occur during the expansion process after a vertex v is added to S, and all vertices in $ext(S)$ that are not within 2-hops of v are removed. The *indeg* and *exdeg* (as in Fig. 4) need to be updated after removal occurs. The vertices whose *indeg* and *exdeg* do not meet the criteria will be removed, prompting another round of degree updates. Thus, degree updates will trigger pruning, and pruning will trigger another round of degree updates. This iterative pruning continues until no vertex can be removed. To efficiently perform this iterative degree-based pruning, we initialize two auxiliary data structures as shown in Fig. 6: *RemainingVertices*, which stores all the vertices not pruned, and *RemovedVertices*, which stores all the vertices that have been pruned. We will discuss the details below.

To perform degree-based pruning, we first need to update the degrees of the remaining vertices via an intersection after vertex removal occurs. This can be done via two methods:

$$\forall v \in RemainingVertices,$$
$$exdeg(v) \leftarrow exdeg(v) - |N_G(v) \cap RemovedVertices|$$

or

$$exdeg(v) \leftarrow |N_G(v) \cap RemainingVertices|$$

Our kernel profiling shows that the intersection above is the most computationally intensive part of the program, due to the potentially large size of all components involved. Each thread handles the degree calculation above for one vertex in the task. We have optimized the intersection by dynamically selecting the most efficient method based on the sizes of *RemainingVertices* and *RemovedVertices*, as the smaller set will result in fewer intersections. Additionally, we preprocess and sort the adjacency list. This allows us to use binary search when searching for neighbors of a vertex in the remaining or removed sets.

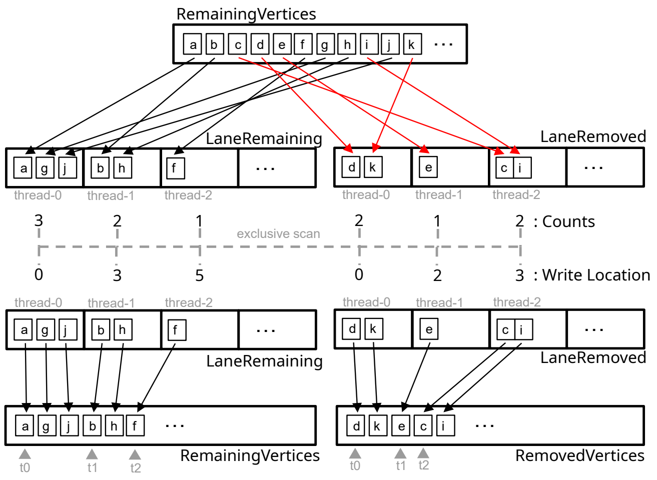

Fig. 6. Parallel Degree-Pruning on GPU

Once the intersection is completed, we have an updated *RemainingVertices*, shown at the top of Fig. 6, where the degrees of the vertices have been updated. With these updated degrees, we can apply degree-based pruning on each vertex. Each time, every thread will process one vertex, applying the degree-based pruning rules to determine its validity. However, we cannot directly write these results back to *RemainingVertices* and *RemovedVertices* due to potential race conditions. To address this, we create two auxiliary buffer structures: *ThreadRemaining* for each thread's remaining vertices and *ThreadRemoved* for removed vertices. As shown by the top arrows in Fig. 6, each thread performs its degree-based pruning and writes to its own buffers, while tracking the count of remaining and removed vertices in its registers.

Using each thread's count of remaining and removed vertices, we perform an exclusive scan across the warp to determine each thread's write location (as t0, t1, t2 in Fig. 6) in *RemaingVertices* and *RemovedVertices*. The exclusive scan is implemented using CUDA warp-level primitives for efficiency. Subsequently, threads consolidate their results from *ThreadRemaing* and *ThreadRemoved* into *RemainingVertices* and *RemovedVertices*, shown by the lower arrows in Fig. 6. Please note that the degree pruning workflow in Fig. 6 will repeat until no more vertices can be removed.

V. GPU Efficiency

The following explains the GPU effectiveness of our system.

Maximizing Utilization. High utilization is achieved by keeping warps continuously busy. Our task-based design generates thousands of independent tasks, ensuring enough work for every warp. Dynamic Task Scheduling balances workloads, preventing idle time by quickly assigning new tasks to finished warps. These systems together maintain consistent work for all of the GPU's warps.

Maximizing Memory Throughput. As explained in Section II, memory access should prioritize registers (fastest but smallest), followed by shared memory, and finally global memory (slowest but largest).

In our program, registers are used for pruning rules, with each lane in the warp pruning a subset of vertices and storing results in registers. After pruning, the warp combines results using efficient warp-level primitive operations, which rely on data exchange between registers.

Shared Memory stores warp-wide variables and facilitates communication. For example, if a warp detects a failed vertex, a shared variable is updated as a communicator to notify all threads to halt for this task. We also have shared-memory buffer to accelerate frequent task accesses when tasks are small.

To ensure efficient retrievals from global memory, we follow the coalesced memory access. Our task data structure, using the CSR data format, stores related information contiguously in a linear array. When lanes access contiguous memory, multiple retrievals are combined into a single access.

Maximizing Instruction Throughput. Low warp-level divergence and efficient operators allow warps to execute more instructions per second. This is accomplished in cuQC by using the efficient warp-level primitive operations for our scan and sum operations during pruning, as discussed in Section IV-G. Additionally, our intersection Design is tailored for warp execution as it reduces conditionals, minimizing divergence.

Minimize Memory Thrashing. Memory thrashing occurs with frequent allocations and deallocations. In our system, memory is allocated and freed only once, with no management between levels, minimizing thrashing.

VI. Distributed Memory

Real-life graphs are typically large and complex, making a single GPU inadequate for their processing. To address this, we developed a multi-GPU version of cuQC to enhance the algorithm's performance. The core concept involves redistributing tasks: once a process completes its assigned tasks, it receives additional tasks from those still in progress.

Distributed Program. The distributed program is presented in Algorithm 3. Line 1 represents the first 12 lines of Algorithm 1, which involve loading the data, performing CPU expansion, and transferring the data to the GPU. Notably, the distributed version still follows the hybrid CPU-GPU design. Enough tasks will be spawned after the CPU stage to feed the GPUs. To balance the workload between multiple GPUs, these tasks are distributed among different GPU nodes in a strided manner, as the early spawned tasks are likely to be larger due

Algorithm 3 Distributed Memory Algorithm 1

Input: $G = (V, E)$
Output: All MQCs

```
1:  Lines 1-12 from Algorithm 1
2:  while !$all\_GPUs\_free()$ do
3:      while $TaskList \neq \emptyset$ and $TaskBuffer \neq \emptyset$ do
4:          Lines 14-21 from Algorithm 1
5:          if $TaskBuffer > \tau_{help}$ then
6:              $send \leftarrow send\_work()$
7:              if $send$ then
8:                  Update $TaskBuffer$
9:              end if
10:         end if
11:     end while
12:     $broadcast\_free(rank)$
13:     $receive \leftarrow receive\_work()$
14:     if $receive$ then
15:         Update $TaskBuffer$
16:         Refill $TaskBuffer$ to $TaskList$
17:         $broadcast\_received(rank)$
18:     end if
19: end while
20: Save $ResultList$ in file
```

to having more candidates. For example, if there are 16 tasks with IDs ranging from 0 to 15 to be assigned among 4 GPUs, GPU-0 receives tasks t_0, t_4, t_8, t_{12}, GPU-1 receives tasks t_1, t_5, t_9, t_{13}, and so on.

Lines 3–11 perform the local GPU expansion of tasks until completion. Specifically, Line 4 corresponds to lines 14–21 of Algorithm 1, which generate the next level of tasks from the current level. Unlike the previous algorithm, at the end of each level, Line 5 checks if *TaskBuffer* exceeds τ_{help}. If so, Line 6 invokes the *send_work()* method, which attempts to send idle tasks to another process and returns whether it is successful. If it is successful, τ_{send} of tasks from *TaskBuffer* will be sent to the receiving process's *TaskBuffer*. The hyperparameter τ_{help} and τ_{send} ensure tasks are sent only when their volume justifies the network communication overhead, which is set by the user based on network speed. Line 7 verifies sending success, and Line 8 updates *TaskBuffer* size accordingly.

Continuing from line 12, all local tasks have been completed, and the focus shifts to obtaining tasks from a process that still has tasks. Initially, a broadcast message is sent to all processes, indicating that this process is now free Line 13 invokes the *receive_work()* method, which attempts to receive work from another process and returns a success status. If task reception was successful, Lines 15–17 update the *TaskBuffer*, fill *TaskList* from *TaskBuffer*, and broadcast to all other processes that this process is no longer free. The communication between multi-GPUs is discussed as follows.

Message Passing. To ensure that one node will send its idle tasks to only one other node, we have designed the communication to follow a "Three-way Handshake" approach. As shown in Fig. 7, when a process becomes free, it broadcasts its status as f to all other processes. The free process will then continuously check for messages from other processes. It will wait until either all processes' statuses become f (indicating the entire program is finished) or one process sends an r (indicating a busy node is requesting help). The free process will respond to the busy node with a c message, asking for confirmation. This confirmation is necessary because, due to the asynchronous design, the requesting process might have completed all its tasks by the time the confirmation message arrives. If the busy process still has tasks, it will reply with C to one idle process, initiating the transfer. When the idle process has received the work, it will broadcast t (taken work), declaring that it is no longer free. If multiple free processes have sent a c, the busy process will send a D (decline) to the others, indicating that it is declining their help, prompting them to continue looking for other requesting processes.

This system is designed to be asynchronous, with all processes being non-blocking except those involved in the actual sending and receiving of tasks. This blocking communication is highlighted in red in Fig. 7. Messages containing vertex data are efficiently transmitted using *MPI_Datatype*. Using *MPI_Datatype*, vertex data is efficiently sent in a single transaction, avoiding the need to send different variables in multiple messages. These designs ensure maximal GPU utilization and guarantee excellent scalability as the number of GPUs increases, as demonstrated in the following experiments.

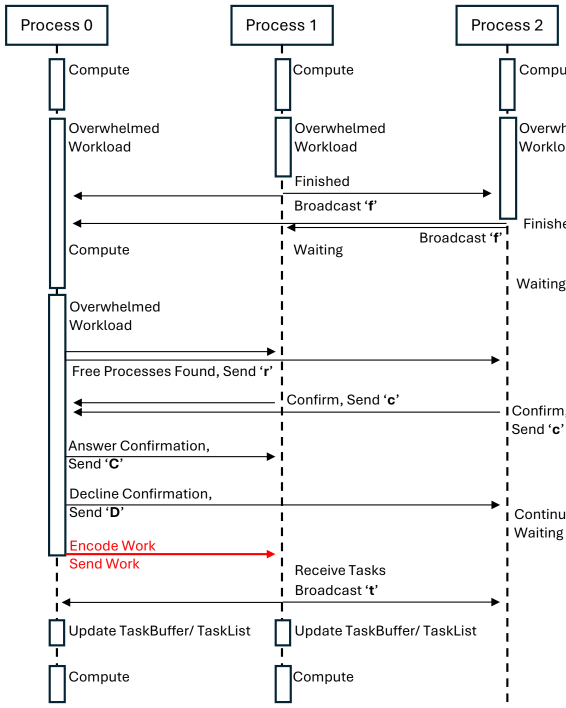

Fig. 7. Distributed GPUs Communication

VII. EXPERIMENTS

In this section, we conduct comprehensive experiments to evaluate the performance of cuQC.

A. Experimental Setup

Platform. We evaluate our GPU implementations on an NVIDIA A100 GPU [30] with 108 streaming multiprocessors

(SMs) and 80 GB of global memory. For the comparison, we run the other CPU-based MQC algorithm T-thinker on a Linux server with AMD EPYC 7763 64-Core Processor @ 2.45GHz CPU cores.

Datasets. We comprehensively evaluate our cuQC algorithm and baselines on 21 public graph datasets with varying sizes and densities. As shown in Table I, the datasets are listed in ascending order of the number of vertices. These datasets span numerous categories, including (1) social networks such as Ego-Facebook [31], LastFM [32], FB-Pages [33], Brightkite [34], Gowalla [35], YouTube [36], Hyves [37], Flixster [38], Livejournal [39], and Konect [40]; (2) collaboration networks such as Ca-GrQc [41], HepPh [42], AstroPh [43], CondMat [44], Citeseer [45], DBLP [46]; (3) biological network CX_GSE1730 [47]; (4) email communication network Enron [48]; (5) a co-purchasing network Amazon [49]; (6) an internet topology Skitter [50]; and (7) a protein k-mer Kmer [51]. The datasets have been frequently used in previous works on serial and parallel clique mining. Some graphs were originally directed but have been made undirected by disregarding edge direction.

TABLE I
GRAPH DATASETS

Dataset	$\|V\|$	$\|E\|$	$\|E\| / \|V\|$	Max Degree
CX_GSE1730	998	5,096	5.11	197
Ego-Facebook	4,039	88,234	21.85	1,045
Ca-GrQc	5,242	14,496	2.77	81
LastFM	7,624	27,806	3.65	216
HepPh	12,008	118,521	9.87	491
AstroPh	18,772	198,110	10.55	504
CondMat	23,133	93,497	4.04	280
Enron	36,692	183,831	5.01	1,383
FB-Pages	50,516	819,306	16.22	1,469
Brightkite	58,228	214,078	3.68	1,134
Gowalla	196,591	950,327	4.83	14,730
Citeseer	227,320	814,134	3.58	1,372
DBLP	317,080	1,049,866	3.31	343
Amazon	334,863	925,872	2.76	549
YouTube	1,134,890	2,987,624	2.63	28,754
Hyves	1,402,673	2,777,419	1.98	31,883
Skitter	1,696,415	11,095,298	6.54	35,455
Flixster	2,523,387	7,918,801	3.14	1,474
Livejournal	4,033,138	27,933,062	6.93	2,651
Konect	59,216,212	92,522,014	1.56	4,960
Kmer	67,716,231	69,389,281	1.02	35

Compared Algorithms. Since there is no existing GPU-accelerated algorithm for MQC, we compare cuQC to CPU-oriented algorithms, including the recent serial version Quick [3], and the cutting-edge parallel MQC algorithm, i.e., parallel Quick+ on T-thinker [21]. To ensure fair comparisons, we execute them on the same platform. Since our machine contains 64 CPU cores, we run the parallel Quick+ with 64 processes using the default settings described in the paper [21].

Measures. We measure the running time of each algorithm, excluding the time spent reading the graph from the disk and the post-processing to remove non-maximal quasi-cliques. By default, cuQC sets the values for τ_{cpu} (rounds ran on CPU) to 2 and uses dynamic scheduling. We also implement other variants to evaluate the techniques proposed in this paper, which will be detailed in the corresponding experiments.

B. Overall Evaluation

We configure a kernel grid to have 216 thread blocks, with each block comprising 1,024 threads. Table II compares the running times of the serial Quick, parallel CPU-based T-thinker, and our GPU-based program cuQC on real-world datasets. The symbol "-" indicates that the program could not complete execution within 24 hours. The experimental results demonstrate that our cuQC can achieve a remarkable 3,992x speedup compared to the serial Quick algorithm when evaluated on the AstroPh dataset. This exceptional acceleration shows the significant performance gains attainable by cuQC through its effective utilization of the massively parallel computing capabilities of the GPU.

Our cuQC can also achieve an impressive 179x speedup over the parallel CPU-based T-thinker system (see Table II). This acceleration effect is significantly observed in dense graphs, exemplified by dataset Ego-Facebook with an average degree of 21.85 and AstroPh with an average degree of 10.55. During the exploration of the set-enumeration tree, these dense graphs spawn a multitude of computationally intensive tasks that cannot be easily pruned. Our GPU system is well-designed for efficiently performing the pruning calculations associated with these demanding tasks, enabling cuQC to outperform both CPU-based competitors by orders of magnitude on such dense graph datasets. Additionally, T-thinker is a task-based graph mining system that flushes tasks onto the disk to maintain bounded memory usage. After two hours of execution on the AstroPh and Ego-Facebook datasets, we had to terminate the T-thinker system, as the generated task files were set to fill our 2 TB disk.

TABLE II
OVERALL EVALUATION

Dataset	γ	τ_{size}	#{MQC}	Quick (ms)	T-thinker (ms)	cuQC (ms)
CX_GSE1730	0.9	30	1,602	191	235	120
Ego-Facebook	0.95	103	2	-	-	230,940
Ca-GrQc	0.8	10	43,399	366	242	199
LastFM	0.75	20	23,319	7,405	5,465	199
HepPh	0.95	71	5	-	-	228
AstroPh	0.8	54	54,772	906,245	40,754	227
CondMat	0.8	15	4,396	835	625	199
Enron	0.9	23	200	127,926	12,813	3,284
FB-Pages	.9	24	17	1,894,457	2,174,848	440,164
Brightkite	0.9	50	1,361	500,637	25,319	374
Gowalla	0.9	30	11	1,073,253	65,037	14,108
Citeseer	0.9	60	26,312	-	1,494	595
DBLP	0.9	73	2	1,540	1660	158
Amazon	0.5	12	13	1,028	1,230	377
YouTube	0.9	18	274	-	898,070	716,804
Hyves	0.9	22	1,480	190,655	109,564	13,846
Skitter	0.95	53	96	-	-	73,875
Flixster	.9	50	49	-	-	53,234
Livejournal	.95	196	56,057	-	-	63,213
Konect	.5	15	25,392	-	-	13,568,398
Kmer	0.5	10	63	49,752	48,215	28,311

Due to space limitations, we are unable to present experiments for all datasets. Instead, we represent the datasets by size. For small graphs ($|V| < 100,000$), we chose Ego-Facebook. For medium graphs ($100,000 \leq |V| \leq 1,000,000$), we selected Gowalla. For large graphs ($|V| > 1,000,000$), we chose Skitter. These graphs were chosen for their high $|V|/|E|$ ratios, ensuring they would present non-trivial challenges.

C. Effect of Optimizations

Static Scheduling v.s. Dynamic Scheduling. To analyze the impact of different task scheduling strategies described in Section IV, we designed two variants of cuQC: a static scheduling version and a dynamic scheduling version. Table III illustrates that the dynamic scheduling strategy significantly accelerates the program's performance, as it promotes workload balancing by assigning the next available task to an idle warp on the GPU immediately, taking full advantage of the GPU's computational resources.

TABLE III
TASK SCHEDULING

Dataset	Static (ms)	Dynamic (ms)	Speedup
Ego-Facebook	254,173	243,744	1.04
Gowalla	17,770	14,293	1.24
Skitter	79.897	74,517	1.07

Shared Memory Buffer. We examine the effect of varying the size of *SharedVertices* through τ_{shared}. As depicted in Table IV, the shared memory buffer does not enhance performance. Since all data produced similar trivial results, we decided to display only the Gowalla dataset test. The performance gain is negligible because the tasks generated by our datasets exceed the limited shared memory capacity. The A100 GPU has 64 KB of shared memory per block, which allocates only 2 KB per warp. Furthermore, some variables shared by warps already occupy part of this memory. As shown in Fig. II and IV, τ_{size} often eclipses τ_{shared}, in these situations *SharedVertices* can never be used. Similar observations have been reported in other GPU-based studies [52] when attempting to optimize systems using shared memory. Additionally, the primary time cost in our system arises from the intersection of vertex adjacency lists, which are required to be stored in global memory due to their size. Therefore, accessing global memory remains essential.

TABLE IV
EFFECT OF SHARED MEMORY BUFFERING

Dataset	τ_{shared}	Time (ms)
Gowalla	0	13,875
	20	13,954
	40	13,956
	60	13,973

D. Sensitivity Analysis

Effect of Hyperparameter. We explore how the mining time varies with MQC problem parameters γ and τ_{size}. We utilize three datasets, Hyves, Gowalla, and Enron, for illustration. We skipped denser datasets like Ego-Facebook because they could generate millions of cliques with certain parameters, preventing proper runs. Since this test aims to illustrate the properties of the problem rather than our system, these three graphs are sufficient. Table V presents the number of results (denoted by $\#\{MQC\}$) found by cuQC, along with the job running time with varying τ_{size} and γ. We observe that even minor changes of τ_{size} or γ can significantly impact the number of results. For instance, when changing (τ_{size}, γ) from $(22, 0.90)$ to $(22, 0.91)$ on Hyves, the results number decreases from 1,480 to 6. Similarly, when fixing γ and incrementing τ_{size} from 21 to 22 for dataset Enron, the number of results decreases substantially, from 20,742 to 2,424. These observations highlight the MQC problem's sensitivity to variations in the input parameters, necessitating careful tuning to obtain the desired number of MQC within reasonable time constraints.

TABLE V
EFFECT OF HYPERPARAMETERS

(a) Effect of γ

Dataset	τ_{size}	γ	Time (ms)	#{MQC}
Hyves	22	0.88	13,488	1,433
		0.89	13,468	1,480
		0.90	13,551	1,480
		0.91	12,277	6
		0.92	12,169	0
Gowalla	30	0.88	16,739	82
		0.89	16,751	82
		0.90	14,103	11
		0.91	15,775	7
		0.92	15,311	7
Enron	23	0.88	3,088	191
		0.89	3,317	200
		0.90	3,299	200
		0.91	2,802	15
		0.92	2,655	0

(b) Effect of τ_{size}

Dataset	τ_{size}	γ	Time (ms)	#{MQC}
Hyves	20	0.9	15,472	11,087
	21		15,450	11,087
	22		13,505	1,480
	23		12,344	114
	24		11,226	6
Gowalla	28	0.9	30,774	113
	29		19,091	24
	30		14,261	11
	31		14,459	11
	32		12,073	1
Enron	21	0.9	4,172	20,742
	22		3,637	2,424
	23		3,314	200
	24		3,104	15
	25		2,901	0

Effect of Expand Threshold. Our system has a configurable setting τ_{expand}, which approximately determines the number of tasks handled by each warp per round. This setting indirectly determines the size of the *WarpTaskBuffer* and *TaskBuffer* containers. As shown in Table VI, this hyperparameter impacts both runtime and memory usage. For instance, by increasing τ_{expand} from $6,912$ ($Warp\#/Block \times BlockNum$) to $691,200$ on Ego-Facebook, the runtime decreases from 582,672 ms to 243,529 ms, while the memory usage increases from 2,003 MB to 18,261 MB.

Increasing τ_{expand} reduces time by activating more tasks in each level kernel call. This decreases the frequency of data transfers between the *WarpTaskBuffer* and *TaskBuffer*, and more active tasks enhance the ability to balance workloads using the dynamic task scheduling strategy. However, it will also increase memory usage since more tasks will generate sub-tasks during the same level kernel call.

We aim to run all graphs with a τ_{expand} of 100, but for the Youtube graph, we use a τ_{expand} of 10 to bound the memory. This hyperparameter enhances the adaptability of our system across different GPUs. For GPUs with limited memory capacity, users can still scale to big graphs by tuning the τ_{expand} setting accordingly. This flexibility enables our system to accommodate a wide range of GPU configurations, facilitating efficient quasi-clique mining on diverse hardware platforms while balancing runtime and memory requirements.

E. Ablation Study

In this experiment, we evaluate the effectiveness of the pruning techniques on the GPU. We selected smaller graphs for these tests because, as without pruning techniques, the

TABLE VI
EFFECT OF EXPAND THRESHOLD

Dataset	τ_{expand}	Time (ms)	Memory (MB)
Ego-Facebook	6,912	582,672	2,003
	13,824	416,515	2,313
	69,120	277,471	4,627
	345,600	247,587	11,327
	691,200	243,529	18,261
Gowalla	6,912	17,173	29,975
	13,824	15,125	29,975
	69,120	14,222	29,975
	345,600	14,492	29,983
	691,200	14,471	29,987
Skitter	6,912	241,715	34,849
	13,824	183,490	35,367
	69,120	106,353	36,509
	345,600	75,355	38,523
	691,200	74,636	42,031

search space is too large, making larger graphs unmanageable. Additionally, diameter and degree-based pruning are fundamental to the program and are included in all algorithms. We implemented a baseline mining algorithm that does not use most pruning techniques described in Section IV. We then add one of the pruning techniques to the baseline GPU algorithm. Table VII presents the running time of the baseline algorithm and pruning techniques on LastFM and Condmat. These results highlight the necessity of assembling all the proposed techniques on the GPU. This is because no single pruning technique exhibits consistent effectiveness across all datasets. For instance, the lookahead technique does not provide significant benefits on the LastFM dataset. However, it achieves a speedup ratio of 24.67 on the Condmat dataset. This implies that the effectiveness of the pruning techniques is dependent on the characteristics of the underlying datasets.

TABLE VII
EFFECTIVENESS OF PRUNING TECHNIQUES ON GPU

Dataset	Algorithm	Time (ms)	Speedup
LastFM	Baseline	4,113	-
	Baseline + Lookahead	3,616	1.14
	Baseline + UpperLower	1,851	2.22
	Baseline + CriticalVertex	2,002	2.05
	cuQC	779	5.28
Condmat	Baseline	27,429	-
	Baseline + Lookahead	1,112	24.67
	Baseline + UpperLower	27,543	1.00
	Baseline + CriticalVertex	26,802	1.02
	cuQC	1,062	25.83

F. Distributed Memory

We evaluate our distributed GPU implementation using 4 NVIDIA A100 GPUs [30], the maximum supported by our cluster.

Datasets. Compared to the single-node version, the distributed version is designed for large graphs where there is sufficient work to utilize all GPUs. Therefore, we ran the following tests on three large, high-density datasets: Ego-Facebook [31], FB-Pages [33], and Konect [40].

Evaluation. Table VIII reports the scalability when we vary the number of GPUs as 1, 2, 3, and 4. We can see that additional machines generally improves the performance. Perfect scalability is impossible due to some parts of the program running on the CPU and the communication overhead between GPUs. The experimental results demonstrate that we can come very close to the ideal scalability on graphs with lots of work. For the 4 GPU version on the Konect graph, we achieved a speedup of 3.9 times compared with a single node.

TABLE VIII
SCALABILITY

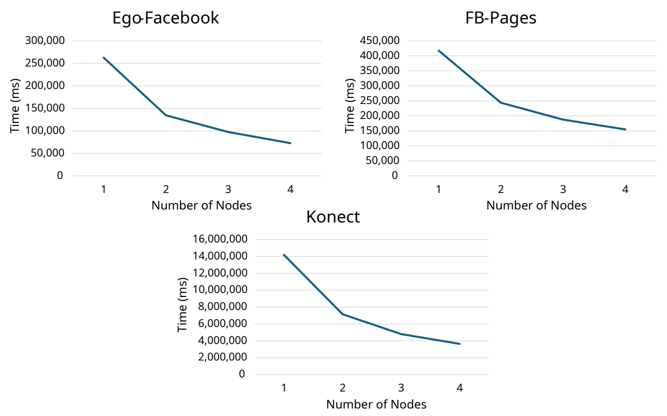

Effect of Help Threshold. In our program, we have a configurable setting, τ_{help}, which specifies the number of remaining tasks at which processes should begin distributing work to other GPUs. A lower τ_{help} means more tasks can be balanced to other idle GPUs from a busy one, but it also induces more communication overhead. Note that our experiment starts with τ_{help} set at $6,912$ to ensure that at least one task is left for each warp. As shown in Table IX, a τ_{help} of the minimum $6,912$ is ideal. This is due to the extremely fast intra-node communication on our server, making messaging times for these larger graphs negligible compared to computation time.

TABLE IX
EFFECT OF HELP THRESHOLD

Dataset	τ_{help}	Time (ms)
Ego-Facebook	6,912	148,201
	13,824	150,674
	69,120	205,089
	345,600	205,016
	691,200	205,100
FB-Pages	6,912	155,779
	13,824	156,903
	69,120	156,329
	345,600	160,851
	691,200	160,143
Konect	6,912	3,640,231
	13,824	3,657,240
	69,120	3,656,189
	345,600	3,642,673
	691,200	3,639,677

VIII. CONCLUSION

We have designed the first highly efficient MQC system on the GPU and a corresponding distributed version. Mining MQC on big graphs using the GPU faces serious challenges, including large memory requirements, thread divergence, and severe load imbalance. To address these problems, novel GPU-aware data structures and optimization techniques are designed on our cuQC. Our experiments show that cuQC significantly outperforms traditional serial CPU solutions and is also faster than parallel CPU solutions. In future work, we plan to generalize this project into a GPU platform that allows users to implement their own graph mining algorithms.

References

[1] Y. Fang, K. Wang, X. Lin, and W. Zhang, "Cohesive subgraph search over big heterogeneous information networks: Applications, challenges, and solutions," in *SIGMOD '21: International Conference on Management of Data, Virtual Event, China, June 20-25, 2021*, G. Li, Z. Li, S. Idreos, and D. Srivastava, Eds. ACM, 2021, pp. 2829–2838.

[2] G. Guo, D. Yan, M. T. Özsu, Z. Jiang, and J. Khalil, "Scalable mining of maximal quasi-cliques: An algorithm-system codesign approach," *Proc. VLDB Endow.*, vol. 14, no. 4, pp. 573–585, 2020.

[3] G. Liu and L. Wong, "Effective pruning techniques for mining quasi-cliques," in *ECML/PKDD*, ser. Lecture Notes in Computer Science, W. Daelemans, B. Goethals, and K. Morik, Eds., vol. 5212. Springer, 2008, pp. 33–49.

[4] M. Bhattacharyya and S. Bandyopadhyay, "Mining the largest quasi-clique in human protein interactome," in *2009 International Conference on Adaptive and Intelligent Systems*. IEEE, 2009, pp. 194–199.

[5] H. Matsuda, T. Ishihara, and A. Hashimoto, "Classifying molecular sequences using a linkage graph with their pairwise similarities," *Theor. Comput. Sci.*, vol. 210, no. 2, pp. 305–325, 1999.

[6] G. D. Bader and C. W. Hogue, "An automated method for finding molecular complexes in large protein interaction networks," *BMC bioinformatics*, vol. 4, no. 1, p. 2, 2003.

[7] D. Bu, Y. Zhao, L. Cai, H. Xue, X. Zhu, H. Lu, J. Zhang, S. Sun, L. Ling, N. Zhang *et al.*, "Topological structure analysis of the protein–protein interaction network in budding yeast," *Nucleic acids research*, vol. 31, no. 9, pp. 2443–2450, 2003.

[8] H. Hu, X. Yan, Y. Huang, J. Han, and X. J. Zhou, "Mining coherent dense subgraphs across massive biological networks for functional discovery," *Bioinformatics*, vol. 21, no. suppl_1, pp. i213–i221, 2005.

[9] D. Ucar, S. Asur, U. Catalyurek, and S. Parthasarathy, "Improving functional modularity in protein-protein interactions graphs using hub-induced subgraphs," in *European Conference on Principles of Data Mining and Knowledge Discovery*. Springer, 2006, pp. 371–382.

[10] J. Li, X. Wang, and Y. Cui, "Uncovering the overlapping community structure of complex networks by maximal cliques," *Physica A: Statistical Mechanics and its Applications*, vol. 415, pp. 398–406, 2014.

[11] J. Hopcroft, O. Khan, B. Kulis, and B. Selman, "Tracking evolving communities in large linked networks," *Proceedings of the National Academy of Sciences*, vol. 101, no. suppl 1, pp. 5249–5253, 2004.

[12] C. Wei, A. Sprague, G. Warner, and A. Skjellum, "Mining spam email to identify common origins for forensic application," in *ACM Symposium on Applied Computing*, R. L. Wainwright and H. Haddad, Eds. ACM, 2008, pp. 1433–1437.

[13] S. Sheng, B. Wardman, G. Warner, L. Cranor, J. Hong, and C. Zhang, "An empirical analysis of phishing blacklists," in *6th Conference on Email and Anti-Spam (CEAS)*. Carnegie Mellon University, 2009.

[14] D. Weiss and G. Warner, "Tracking criminals on facebook: A case study from a digital forensics reu program," in *Proceedings of Annual ADFSL Conference on Digital Forensics, Security and Law*, 2015.

[15] S. Sanei-Mehri, A. Das, and S. Tirthapura, "Enumerating top-k quasi-cliques," in *IEEE BigData*. IEEE, 2018, pp. 1107–1112.

[16] G. Pastukhov, A. Veremyev, V. Boginski, and O. A. Prokopyev, "On maximum degree-based γ-quasi-clique problem: Complexity and exact approaches," *Networks*, vol. 71, no. 2, pp. 136–152, 2018. [Online]. Available: https://doi.org/10.1002/net.21791

[17] J. Pei, D. Jiang, and A. Zhang, "On mining cross-graph quasi-cliques," in *SIGKDD*. ACM, 2005, pp. 228–238.

[18] D. Jiang and J. Pei, "Mining frequent cross-graph quasi-cliques," *ACM Trans. Knowl. Discov. Data*, vol. 2, no. 4, pp. 16:1–16:42, 2009.

[19] Z. Zeng, J. Wang, L. Zhou, and G. Karypis, "Coherent closed quasi-clique discovery from large dense graph databases," in *SIGKDD*. ACM, 2006, pp. 797–802.

[20] K. Yu and C. Long, "Fast maximal quasi-clique enumeration: A pruning and branching co-design approach," *Proc. ACM Manag. Data*, vol. 1, no. 3, pp. 211:1–211:26, 2023. [Online]. Available: https://doi.org/10.1145/3617331

[21] J. Khalil, D. Yan, G. Guo, and L. Yuan, "Parallel mining of large maximal quasi-cliques," *VLDB J.*, vol. 31, no. 4, pp. 649–674, 2022. [Online]. Available: https://doi.org/10.1007/s00778-021-00712-2

[22] A. Quamar, A. Deshpande, and J. Lin, "Nscale: neighborhood-centric large-scale graph analytics in the cloud," *The VLDB Journal*, pp. 1–26, 2014.

[23] C. H. C. Teixeira, A. J. Fonseca, M. Serafini, G. Siganos, M. J. Zaki, and A. Aboulnaga, "Arabesque: a system for distributed graph mining," in *SOSP*, 2015, pp. 425–440.

[24] H. Chen, M. Liu, Y. Zhao, X. Yan, D. Yan, and J. Cheng, "G-miner: an efficient task-oriented graph mining system," in *Proceedings of the Thirteenth EuroSys Conference, EuroSys 2018, Porto, Portugal, April 23-26, 2018*, R. Oliveira, P. Felber, and Y. C. Hu, Eds. ACM, pp. 32:1–32:12.

[25] D. Yan, G. Guo, M. M. R. Chowdhury, T. Özsu, W.-S. Ku, and J. C. Lui, "G-thinker: A distributed framework for mining subgraphs in a big graph," in *ICDE*, 2020.

[26] M. Valiyev, "Graph storage: How good is csr really?" *dated Dec*, vol. 10, p. 8, 2017.

[27] J. L. Greathouse and M. Daga, "Efficient sparse matrix-vector multiplication on gpus using the CSR storage format," in *International Conference for High Performance Computing, Networking, Storage and Analysis, SC 2014, New Orleans, LA, USA, November 16-21, 2014*, T. Damkroger and J. J. Dongarra, Eds. IEEE Computer Society, 2014, pp. 769–780.

[28] Y. Wei, W. Chen, and H. Tsai, "Accelerating the bron-kerbosch algorithm for maximal clique enumeration using gpus," *IEEE Trans. Parallel Distributed Syst.*, vol. 32, no. 9, pp. 2352–2366, 2021.

[29] L. Xiang, A. Khan, E. Serra, M. Halappanavar, and A. Sukumaran-Rajam, "cuts: scaling subgraph isomorphism on distributed multi-gpu systems using trie based data structure," in *International Conference for High Performance Computing, Networking, Storage and Analysis, SC 2021, St. Louis, Missouri, USA, November 14-19, 2021*, B. R. de Supinski, M. W. Hall, and T. Gamblin, Eds. ACM, 2021, p. 69.

[30] "NVIDIA A100 Tensor Core GPU," https://www.nvidia.com/en-gb/data-center/a100/.

[31] "Ego-Facebook," https://snap.stanford.edu/data/ego-Facebook.html.

[32] "LastFM," https://snap.stanford.edu/data/feather-lastfm-social.html.

[33] "FB-Pages-Artist," https://networkrepository.com/fb-pages-artist.php.

[34] "Brightkite," https://snap.stanford.edu/data/loc-Brightkite.html.

[35] "Gowalla," https://snap.stanford.edu/data/loc-Gowalla.html.

[36] "YouTube," https://snap.stanford.edu/data/com-Youtube.html.

[37] "Hyves," http://konect.cc/networks/hyves/.

[38] "Flixster," https://networkrepository.com/soc-flixster.php.

[39] "Livejournal," https://networkrepository.com/soc-livejournal.php.

[40] "Konect," https://networkrepository.com/socfb-konect.php.

[41] "Ca-GrQc," https://snap.stanford.edu/data/ca-GrQc.html.

[42] "HepPh," https://snap.stanford.edu/data/ca-HepPh.html.

[43] "AstroPh," https://snap.stanford.edu/data/ca-AstroPh.html.

[44] "CondMat," https://snap.stanford.edu/data/ca-CondMat.html.

[45] "Citeseer," https://networkrepository.com/ca-citeseer.php.

[46] "DBLP," https://snap.stanford.edu/data/com-DBLP.html.

[47] "CX_GSE1730," https://www.ncbi.nlm.nih.gov/geo/query/acc.cgi?acc=GSE1730.

[48] "Enron," https://snap.stanford.edu/data/email-Enron.html.

[49] "Amazon," https://snap.stanford.edu/data/com-Amazon.html.

[50] "Skitter," https://snap.stanford.edu/data/as-Skitter.html.

[51] "Kmer," https://graphchallenge.s3.amazonaws.com/synthetic/gc6/U1a.tsv.

[52] A. Ahmad, L. Yuan, D. Yan, G. Guo, J. Chen, and C. Zhang, "Accelerating k-core decomposition by a GPU," in *39th IEEE International Conference on Data Engineering, ICDE 2023, Anaheim, CA, USA, April 3-7, 2023*. IEEE, 2023, pp. 1818–1831.